The Astrophysical Journal, 810:87 (9pp), 2015 September 10 doi:10.1088/0004-637X/810/2/87

SAUSAGE WAVES IN TRANSVERSELY NONUNIFORM MONOLITHIC CORONAL TUBES

I. Lopin[1] and I. Nagorny[2,3]
[1] Ussuriisk astrophysical observatory, Russion Academy of Sciences, Russia; lopin78@mail.ru
[2] Institute of Automation and Control Processes FEB RAS, Vladivostok, Russia
[3] Far Eastern Federal University, Vladivostok, Russia
Received 2015 May 17; accepted 2015 July 17; published 2015 September 2

ABSTRACT

We investigate fast sausage waves in a monolithic coronal magnetic tube, modeled as a local density inhomogeneity with a continuous radial profile. This work is a natural extension of our previous results, obtained for a slab loop model for the case of cylindrical geometry. Using Kneser's oscillating theorem, we provided the criteria for the existence of trapped and leaky wave regimes as a function of the profile features. For a number of density profiles there are only trapped modes for the entire range of longitudinal wave numbers. The phase speed of these modes tends toward the external Alfvén speed in the long wavelength limit. The generalized results were supported by the analytic solution of the wave equation for the specific density profiles. The approximate Wentzel–Kramers–Brillouin solutions allowed us to obtain the desired dispersion relations and to study their properties as a function of the profile parameters. The multicomponent quasi-periodic pulsations in flaring loops, observed on 2001 May 2 and 2002 July 3, are interpreted in terms of the transversely fundamental trapped fast sausage mode with several longitudinal harmonics in a smooth coronal waveguide.

Key words: Sun: helioseismology – Sun: oscillations

1. INTRODUCTION

Coronal loops are the main observational feature of the magnetic structure in the upper solar atmosphere. These structures exist as field-aligned density inhomogeneities in the low-β coronal plasma. Such coronal magnetic tubes are waveguides for a number of magnetohydrodynamic (MHD) waves, e.g., the kink, sausage, torsional, and slow modes (Zaitsev & Stepanov 1982; Edwin & Roberts 1983). Sausage modes are symmetric tube modes ($m = 0$) that produce perturbations in density and magnetic field strength, and the corresponding plasma motions cause pulsations in the tube cross-section (Roberts et al. 1984; Moreels et al. 2013). Generally, sausage waves have both longitudinal and radial wave number vector components. The dominance of the first or a second component ultimately determines the dispersion properties of the sausage mode (i.e., the properties of corresponding oscillations are determined by the loop length or its width). These waves mainly propagate along the uniform and straight magnetic field of the tube. They may possess a stationary (propagating) or evanescent wave structure in the radial direction. The above characteristics correspond to either leaky or trapped wave regimes (Zaitsev & Stepanov 1975; Spruit 1982; Edwin & Roberts 1983; Cally 1986).

The observed manifestations of sausage waves in coronal tubes are caused by plasma compression and the corresponding variations of the magnetic field strength, which lead to modulation of the optical, microwave, gamma-ray, and X-ray emissions. That is why the widely detected phenomena, known as quasi-periodic pulsations (QPP), in flare events are interpreted in terms of fast-sausage pulsations of the coronal magnetic tubes (Rosenberg 1970; Zaitsev & Stepanov 1975; Roberts et al. 1984; Nakariakov et al. 2003; Melnikov et al. 2005; Srivastava et al. 2008; Nakariakov & Melnikov 2009).

The theory of MHD pulsations in a cylindrical model of coronal plasma tubes with a discontinuous density profile was developed by Zaitsev & Stepanov (1982), Edwin & Roberts (1983), and Kopylova et al. (2007). Analytic results indicate that the cutoff wave number, separating the trapped and leaky modes, depends on the tube geometry (viz. its radius) and the values of the Alfvén speed inside and outside the waveguide. The modes with wave numbers below the cutoff value have a temporally decaying amplitude due to the wave leakage effect. On the other hand, the waves with wave numbers above the cutoff are trapped by the waveguide (Zaitsev & Stepanov 1975; Meerson et al. 1978; Roberts et al. 1984; Cally 1986). The main dispersive feature is that the oscillation frequency depends on the radius of a loop in the long wavelength limit, while it depends on the loop length for the short wavelength limit. The decaying decrement of the leaky sausage modes, as was confirmed by Vasheghani Farahani et al. (2014), is linearly proportional to the density contrast (i.e., the ratio of external to internal density). These properties have a crucial role for the methods of coronal seismology, and they allow us to estimate physical parameters in the solar corona.

Objectively, the classical approximation of coronal loops as magnetic flux tubes with a density discontinuity at their boundary is an ideal model. A more realistic case must include the presence of a transition layer with a density which continuously decreases from the internal value to the value in the ambient medium. Alternatively, the monolithic tube model with a continuous density profile can be considered. Therefore, these models take into account the effect of the smoothness of the tube boundary on the dispersion properties of the fast-sausage waves. Edwin & Roberts (1988) carried out a mainly qualitative analysis of the sausage wave properties in the transversely non-uniform waveguides in Cartesian and cylindrical geometries. Nakariakov & Roberts (1995) and Cooper et al. (2003) considered the case of a slab loop model with an Epstein density profile. They found that the presence of a diffuse boundary results in a slight reduction of the corresponding cutoff wavelength, but the basic properties of the modes are the same as those in a model with a discontinuous boundary. Hornsey et al. (2014) performed a

numerical simulation of sausage modes for a model of a coronal slab with an exponent-like Alfvén speed distribution across a loop, while Nakariakov et al. (2012) studied the corresponding cylindrical case. The numerical results are in agreement with the previously obtained analytical data and indicate that the wave frequency is almost independent of the wave number for the long wavelength limit. On the other hand, the wave frequency increases as the wavelength decreases for the short wavelength range. The corresponding phase speed becomes unbounded for the infinitely small wave numbers, and it is located in the neighborhood of the internal Alfvén speed for the large wave numbers.

Nevertheless, the available analytic results encounter some difficulties when attempting to explain the period ratio of the spectral components and the high quality of the multiperiodic QPPs observed in a flaring loops. Indeed, for a characteristic coronal loop, with a length much greater than its width, the fundamental sausage mode is leaky and suffers from strong acoustic damping. Nakariakov et al. (2003) suggested an extremely low density contrast in flaring loops to overcome this problem. Khongorova et al. (2012) considered the particular case of a structured loop model with an external shell where the magnetic field is purely azimuthal. They showed that the fundamental fast-sausage mode remains trapped even in the long wavelength limit. Lopin & Nagorny (2014) studied the radially structured loop model, including a uniform core surrounded by a transition region with density decreasing as an inverse-quadratic function of a radial distance. It was determined that the leaky fundamental fast-sausage mode has a phase speed located in the upper vicinity of the external Alfvén speed in the long wavelength range for the case of a thick transition layer (i.e., diffuse boundary). The damping decrement of this fundamental mode can be rather small to explain the high quality of the observed QPPs. Recently, we provided some analytical reasoning indicating the possible existence of trapped modes in the monolithic smooth coronal slabs over the entire range of longitudinal wave numbers (Lopin & Nagorny 2015). Besides, in the model of a plasma cylinder with a discontinuous density profile, the fast-sausage modes possess high dispersion in the range of wave numbers slightly above and below the cutoff value. This feature significantly complicates the interpretation of the measured period ratio of the spectral components in the detected multiple periodicities in flaring loops (Melnikov et al. 2005; Srivastava et al. 2008; Kupriyanova et al. 2013). Thus, we conclude that studies of the dispersion properties of fast-sausage waves in smooth coronal waveguides are of particular scientific interest, with the goal of obtaining a convincing explanation for the observed data.

The present work is a continuation of our previous investigation of the fast-sausage pulsations in slab-like coronal loops, modeled as smooth density inhomogeneities with a continuous profile (Lopin & Nagorny 2015). We extend our previous results to the case of cylindrical geometry, which seems to be more appropriate to describe the spatial structure of the loops.

2. STATEMENT OF THE PROBLEM

We consider a coronal loop as a density enhancement formed by a magnetic tube with a transverse density profile $\rho(r)$. The plasma space is permeated by the uniform magnetic field, oriented along the z-axis $\boldsymbol{B} = B\boldsymbol{e}_z$, where $\boldsymbol{e}_z$ is a unit longitudinal vector in cylindrical coordinates. We use the approximation of cold plasma ($\beta = 0$), corresponding to the magnetic force domination (i.e., Lorentz force) in the solar corona. Thus, we study only fast magnetoacoustic waves, while the slow modes degenerate. The basic set of MHD equations for the cold plasma limit reads

$$\rho\frac{\partial^2\boldsymbol{\xi}}{\partial t^2} = \frac{\boldsymbol{B}}{\mu_0}\times(\nabla\times\boldsymbol{b}), \tag{1}$$

$$\boldsymbol{b} = \nabla\times(\boldsymbol{\xi}\times\boldsymbol{B}), \tag{2}$$

where $\boldsymbol{\xi} = (\xi_r, \xi_\phi)$ and $\boldsymbol{b} = (b_r, b_\phi, b_z)$ are plasma displacements and magnetic field perturbations. The unperturbed parameters are uniform along the z-axis and azimuthal angle ϕ. Therefore, we can use the Fourier transformation in coordinate z, ϕ, and time t for fluctuating variables, i.e. $\propto \boldsymbol{e}^{-i(\omega t - kz - m\phi)}$. Then Equations (1) and (2) can be reduced to two first-order differential equations in terms of the radial plasma displacements ξ_r and total pressure perturbations $p_T' = \frac{1}{4\pi}(\boldsymbol{B}\cdot\boldsymbol{b})$ (Appert et al. 1974; Sakurai et al. 1991).

$$D\frac{d}{dr}(r\xi_r) = -Crp_T', \tag{3}$$

$$\frac{dp_T'}{dr} = D\xi_r, \tag{4}$$

where

$$D = \rho\left(\omega^2 - V_A^2k^2\right), \tag{5}$$

$$C = \frac{\omega^2}{V_A^2} - k^2 - \frac{m^2}{r^2},\ V_A^2 = \frac{B^2}{4\pi\rho}, \tag{6}$$

and V_A is the Alfvén speed. Equations (3) and (4) can be combined to obtain a single equation in terms of the radial plasma displacements

$$\frac{\partial^2\xi_r}{\partial r^2} + \left(\frac{1}{r} - \frac{C}{D}\frac{\partial}{\partial r}\frac{D}{C}\right)\frac{\partial\xi_r}{\partial r} + \left(C + \frac{1}{r}\frac{C}{D}\frac{\partial}{\partial r}\frac{D}{C} - \frac{1}{r^2}\right)\xi_r = 0, \tag{7}$$

which, in turn, can be converted to the standard form by substitution

$$\xi_r = \Xi_r\exp\left(-\frac{1}{2}\int_r W(r')dr'\right), \tag{8}$$

where

$$W(r) = \frac{1}{r} - \frac{C}{D}\frac{\partial}{\partial r}\frac{D}{C}. \tag{9}$$

The resulting equation is

$$\frac{\partial^2\Xi_r}{\partial r^2} + \left(C - \frac{W}{r} - \frac{W^2}{4} - \frac{1}{2}\frac{\partial W}{\partial r}\right)\Xi_r = 0. \tag{10}$$

Equations (3) and (10), with appropriate boundary conditions, fully describe the behavior of fast waves in radially nonuniform coronal magnetic tubes.

Equations for nonaxisymmetric fast waves with $m = 1, 2\ldots$ in cylindrical geometry contain coefficients with singularities. This feature is due to the radial inhomogeneities of the plasma structure, and it leads to resonant absorption of $m = 1$ kink modes (e.g., Goossens et al. 2002, 2006, 2009; Ruderman &

Roberts 2002; Srivastava & Goossens 2013). The latter effect is not the topic of the present study, and we restrict our attention to the fast-sausage waves only. For axisymmetric modes with $m = 0$, we have $W(r) = r^{-1}$, and Equation (10) simplifies to

$$\frac{\partial^2 \Xi_r}{\partial r^2} + \left(\frac{\omega^2}{V_{\rm A}^2(r)} - k^2 - \frac{3}{4r^2} \right) \Xi_r = 0. \quad (11)$$

3. MONOLITHIC TUBE MODEL

The monolithic model represents the coronal loop as a cold plasma ($\beta = 0$) density enhancement with a continuous radial density profile $\rho(r)$ given by

$$\rho(r) = \rho_e + (\rho_i - \rho_e) f(r), \quad (12)$$

where ρ_i is the density at the axis of the tube, ρ_e is the density at infinity $r \to \infty$, $f(r)$ is a monotonically decreasing continuous function, and $f(0) = 1$, $f(r) \to 0$ as $r \to \infty$. Substituting Equation (12) in Equation (11), we arrive at

$$\frac{\partial^2 \Xi_r}{\partial r^2} + \left(m_e^2 + M_i^2 f(r) - \frac{3}{4r^2} \right) \Xi_r = 0, \quad (13)$$

where

$$m_e^2 = \frac{\omega^2}{V_{\rm Ae}^2} - k^2, \quad M_i^2 = \frac{\omega^2}{V_{\rm Ai}^2}(1 - \chi), \quad \chi = \frac{\rho_e}{\rho_i}. \quad (14)$$

The solution of Equation (13) must be bounded at $r \to \infty$, while at the tube axis $r = 0$ the boundary condition reads

$$\xi_r(r = 0) = 0, \quad (15)$$

corresponding to the plasma motions, which are symmetric with respect to the tube axis.

3.1. Kneser's Oscillation Theorem and Cutoff Wave Numbers

The oscillatory and non-oscillatory solutions of Equation (13) in a nonuniform medium can be distinguished by a known Kneser's oscillation theorem (Kahn 1990; Kneser 1893; see also Musielak & Moore 1995; Schmitz & Fleck 1998; Lopin & Nagorny 2013). It reads that

$$\frac{\partial^2 y}{\partial x^2} + g(x) y = 0 \quad (16)$$

has non-oscillating solutions as $x \to \infty$ if

$$\lim_{x \to \infty} x^2 g(x) \leqslant \frac{1}{4}, \quad (17)$$

and oscillating solutions as $x \to \infty$ for the case

$$\lim_{x \to \infty} x^2 g(x) > \frac{1}{4}. \quad (18)$$

This theorem is based on a comparison of Equation (16) and Euler's equation with the well-known solutions. Direct application of the oscillation theorem to the wave Equation (13) leads to the well-known condition $m_e^2 > 0$ for oscillatory solutions, while the condition $m_e^2 \leqslant 0$ corresponds to non-oscillatory (evanescent) solutions in the uniform medium (Spruit 1982; Edwin & Roberts 1983).

The properties of wave Equation (13) at the critical cutoff point should be considered separately. At the cutoff position, the wave phase speed is equal to the Alfvén speed outside the loop, i.e., we can write

$$\omega_c = V_{\rm Ae} k_c. \quad (19)$$

This critical point separates the trapped and leaky modes. Here, k_c is a cutoff wave number. Equation (13) then reduces to

$$\frac{\partial^2 \Xi_r}{\partial r^2} + \left(M_{ic}^2 f(r) - \frac{3}{4r^2} \right) \Xi_r = 0, \quad (20)$$

where

$$M_{ic}^2 = \frac{1 - \chi}{\chi} k_c^2. \quad (21)$$

Since the wave phase speed is equal to the external Alfvén speed at the cutoff point, the solution of Equation (20) is oscillating everywhere, excluding the infinitely distant points at $r \to \infty$, where $V_{\rm ph} = \omega/k = V_{\rm A}(\infty) = V_{\rm Ae}$. Then, the condition of the non-oscillatory solution at $r \to \infty$ leads to the next constraint,

$$\lim_{r \to \infty} \left(M_{ic}^2 f(r) - \frac{3}{4r^2} \right) \leqslant \frac{1}{4r^2}, \quad (22)$$

and the cutoff wave number limitation is

$$k_c^2 \leqslant \frac{\chi}{1 - \chi} \lim_{r \to \infty} \frac{1}{r^2 f(r)}. \quad (23)$$

The inequality given by Equation (23) yields that when

$$r^2 f(r) \to 0, \quad (24)$$

as $r = \infty$, we have $k_c^2 \leqslant \infty$, i.e., there are a variety of cutoff wave numbers for fast sausage modes. The function $f(r)$, decreasing faster than r^{-2} at large distances from the tube axis, satisfies Equation (24). The opposite condition is

$$r^2 f(r) \to \infty, \quad (25)$$

as $r \to \infty$ corresponds to

$$k_c^2 \leqslant 0, \quad (26)$$

and the fast-sausage modes are trapped for the entire range of wave numbers. Equation (25) is fulfilled if the functions $f(r)$ decrease slower than r^{-2} in the region $r \to \infty$. The intermediate case

$$r^2 f(r) \to D^2 \quad (27)$$

at $r \to \infty$, where D is a positive constant, leads to the condition

$$k_c^2 \leqslant \frac{\chi}{1 - \chi} \frac{1}{D^2}, \quad (28)$$

which corresponds to the single value or a finite set of cutoffs. Equation (27) determines the family of functions for $f(r)$, which decreases like the inverse-quadratic function at $r \to \infty$. The above reasoning is the idealized mathematical relations. Practically, Equation (23) can be applied at large finite distances from the tube axes, in particular at $r \gg r_0$, where r_0 is the effective radius of the density inhomogeneity.

Thus, we can conclude that fast-sausage waves in cylindrical waveguides have the same constraints imposed on the cutoff wave numbers as in a slab model, and this restriction only depends on the behavior of the profile function $f(r)$. This is the expected result because cylindrical Equation (7) can be easily

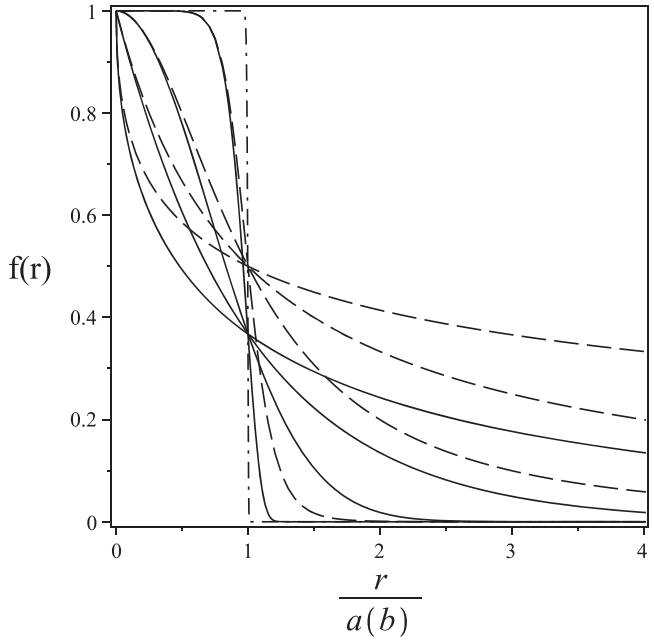

Figure 1. Radial density profile for the monolithic tube model, represented by the profile function $f(r)$. The solid curves correspond to the exponent-like function $f(r)$, calculated for index $\alpha = 1/2$, 1, 2, and 10. The dashed lines are obtained for the inverse polynomial function $f(r)$ with index $n = 1/2$, 1, 2, and 10, and the dashed–dotted line displays the discontinuous profile function.

transformed to the standard form, given by Equation (10), using the appropriate change of variable (see Equation (8)), and this standard form is absolutely identical to the structure of the wave equation in Cartesian geometry.

The obtained results can be illustrated by the example of a density profile function in the form of an inverse polynomial

$$f(r) = \frac{b^n}{b^n + r^n}, \tag{29}$$

where b is the characteristic radius (semiwidth) of inhomogeneity, and the index n characterizes the decreasing rate of the profile (see Figure 1). For index $0 < n < 2$, the function $f(r)$ meets the condition in Equation (25), and all radial modes of fast-sausage waves are trapped for any longitudinal wave numbers. If $n > 2$, then the condition given by Equation (24) is satisfied, and there is a infinite set of cutoffs for sausage modes. When $n = 2$, the condition in Equation (27) is at work, and we have the restriction on the cutoff given by Equation (28) with $D^2 = b^2$. On the other hand, we can obtain the solution of Equation (20) for the considered density profile with $n = 2$ at a large distance from the tube axis $r \gg b$, which reads $\Xi_r(r) = A\sqrt{r}\,\sin\left(\sqrt{M_{ic}^2 b^2 - 1}\,\ln(r)\right)$. As $r \to \infty$, the solution at the cutoff point should be non-oscillatory. With the condition Equation (28), the only possible case is $M_{ic} b \to +1$, and we have

$$k_c^2 b^2 = \frac{\chi}{1-\chi}. \tag{30}$$

The cutoff wave number given by Equation (30) is the same for all fast-sausage modes of arbitrary transverse order. It deviates from the cutoff for a slab model (Lopin & Nagorny 2015) by a numeric factor, and this result is caused only by the difference in the geometries applied.

These findings indicate that, as in the slab geometry, the properties of fast-sausage waves strongly depend on the type of radial density profile in the cylindrical coronal tubes.

3.2. Wentzel–Kramers–Brillouin (WKB) Approximation

For the density contrast $\chi \ll 1$, the WKB method can be applied to obtain the approximate solution of wave Equation (13), which reads (Bender & Orszag 1978)

$$\Xi_r(r) = \exp\left[\frac{1}{\delta}\sum_{l=0}^{\infty}\delta^l S_l(r)\right], \tag{31}$$

where $\delta = \sqrt{\chi}$ is a small parameter. The leading-order terms, corresponding to $l = 0$, 1, then give the first-order WKB-approximation for the solution of Equation (13), which can be written as

$$\Xi_r(r) \approx [-Q(r)]^{-1/4}\left(A\exp\left[\frac{1}{\sqrt{\chi}}\int_r\sqrt{-Q(y)}\,dy\right] + B\exp\left[-\frac{1}{\sqrt{\chi}}\int_r\sqrt{-Q(y)}\,dy\right]\right). \tag{32}$$

Here, A and B are arbitrary constants, and

$$Q(r) = \left(m_e^2 + k^2\right)f(r) + m_e^2\chi - \frac{3\chi}{4r^2}. \tag{33}$$

The WKB approximation is valid if the condition (Bender & Orszag 1978)

$$\frac{1}{\sqrt{\chi}}\int_r\sqrt{-Q(y)}\,dy \gg -\frac{1}{4}\ln(Q(r)), \tag{34}$$

is fulfilled. Equation (34) determines the appropriate range of r, where the expansion, given by Equation (31), is asymptotic in δ.

3.2.1. Cutoffs

At the cutoff point ($m_e = 0$), Equation (33) reads

$$Q_c(r) = k_c^2 f(r) - \frac{3\chi}{4r^2}. \tag{35}$$

Equation (35) yields $Q_c \to -\infty$ as $r \to 0$ and $Q_c \to -0$ as $r \to \infty$. These conditions mean that there are two turning points, where $Q_c = 0$ for the profile functions, satisfying the condition given by Equation (24). The analytic representations for the turning points r_{1c} and r_{2c} are quite complicated, and they depend on the type of the profile function. However, we can give a fairly accurate expression for the first turning point, which is localized in the vicinity of the tube axis $r \approx 0$ (for $\chi \ll 1$), where $f(r) \approx 1$:

$$r_{1c}^2 \approx \frac{3\chi}{4k_c^2}. \tag{36}$$

By analogy with the reasoning in Bender & Orszag (1978), we impose the eigenvalue condition for the two-turning-point

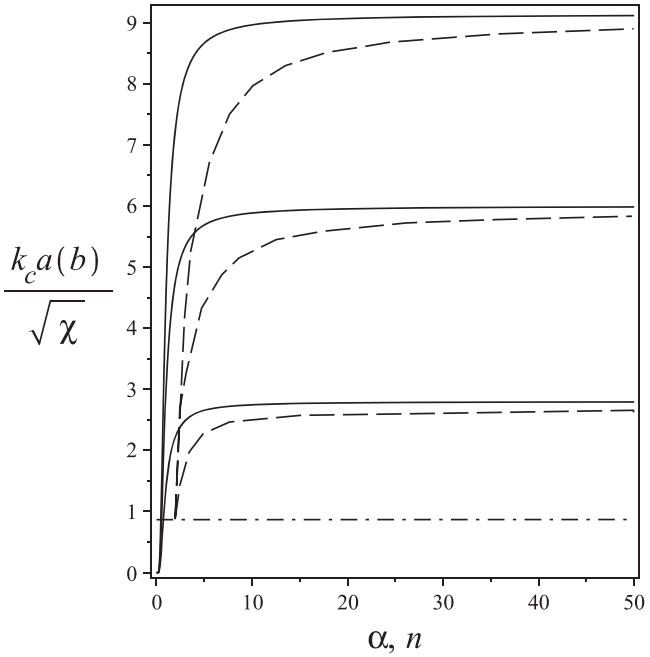

Figure 2. Cutoff wave number dependence of the fundamental, first, and second radial harmonics ($l = 0, 1, 2$) of the fast-sausage mode against the indexes n and α of the profile function $f(r)$. The solid curves represent the exponent-like profile function, and the dashed ones are plotted for the inverse polynomial profile function. The dashed–dotted line corresponds to the WKB approximation of the cutoff value, given by Equation (30).

problem, resulting in the next constraint

$$\frac{1}{\sqrt{\chi}}\int_{r_{1c}}^{r_{2c}}\sqrt{Q_c(r)}\,dr = \pi\left(l+\frac{1}{2}\right). \tag{37}$$

Using Equation (35), we can rewrite Equation (37) as

$$\frac{k_c}{\sqrt{\chi}}\int_{r_{1c}}^{r_{2c}}\sqrt{f(r)-\frac{3\chi}{4k_c^2 r^2}}\,dr = \pi\left(l+\frac{1}{2}\right). \tag{38}$$

Equation (38) gives an implicit expression for the desired cutoff wave numbers. It can be investigated analytically or numerically for the particular cases of the profile function $f(r)$, given that r_{1c} and r_{2c} depend on the cutoff wave numbers.

Let us consider a profile function of the form

$$f(r) = \exp\left[-\left(\frac{r}{a}\right)^{\alpha}\right]. \tag{39}$$

This function, determining the Alfvén speed distribution, was applied by Nakariakov et al. (2012) for a numerical study of the fast-sausage waves in coronal tubes. In Equation (39), parameter α determines the steepness of the density profile, and $2a$ is the transverse size of an inhomogeneity (see Figure 1).

It is easy to show that the first zero r_{1c} of $Q_c(r)$ for the profile function considered can be represented as $r_{1c}^2 = [(3\chi)/(4\delta)]k_c^{-2}$, with $\delta \approx \exp\left[-(3\chi(k_c a)^{-2}/4)^{\alpha/2}\right]$. It follows that $\delta \approx 1$ for not too small α. Then we obtain $r_{1c}/a \ll 1$ if $\chi \ll 1$. Given Equations (35) and (39), we can write the implicit relation for the second turning point in the form

$$r_{2c} = \left(-\ln\left[\frac{3\chi}{4k_c^2 r_{2c}^2}\right]\right)^{1/\alpha} a. \tag{40}$$

As follows from Equation (40), $r_{2c} \to \infty$ as $\alpha \to 0$ and $r_{2c} \to a$ as $\alpha \to \infty$. We can obtain a fairly accurate analytic solution of Equation (38), given that the second term of the integrand is much smaller than the first one because $\chi \ll 1$. By using the Taylor expansion of the integrand on this small term, and taking into account up to the second-order term, we arrive at the resulting cutoff relation

$$k_c a \approx \sqrt{\chi}\,\frac{\alpha}{2^{1/\alpha}\left[\Gamma(1/\alpha) - \Gamma\left(1/\alpha,\,(1/2)(r_{2c}/a)^{\alpha}\right)\right]} \times\left[\pi\left(l+\frac{1}{2}\right)+\frac{2+\delta}{2\sqrt{\delta}}\sqrt{\frac{3}{4}}\right]. \tag{41}$$

It can be shown that $\Gamma(1/\alpha) \gg \Gamma(1/\alpha,\,(1/2)(r_{2c}/a)^{\alpha})$ over the entire range of index α. Equation (41) is similar to that obtained by Lopin & Nagorny (2015) for the smooth plasma slab model, and it gives the dependence of the cutoff wave numbers on the steepness of the tube boundary (by the parameter α). The α-dependent factor in Equation (41) tends to unity from below as $\alpha \to \infty$. This result indicates that the coronal tubes with steeper boundaries (correspond to larger values of α) have higher values of the corresponding cutoffs. Direct comparison of Equation (41) for $\alpha \to \infty$ with the well-known dispersion relation for the step-function density profile (Roberts et al. 1984) demonstrates good agreement, especially for $l \gg 1$, i.e., for high transverse order modes. As follows from Equations (34) and (37), the accuracy of the WKB approximation grows as l increases. Note that $k_c \to 0$ as $\alpha \to 0$ because, in this case, the profile function considered satisfies the condition according to Equation (25).

The same procedure can be applied to the inverse polynomial profile function given by Equation (29). The resulting relation for the cutoff wave numbers reads

$$k_c \approx \frac{\sqrt{\chi}}{r_{2c}F\left(1/2,\,1/n,\,1+1/n,\,-(r_{2c}/b)^n\right) - g(r_{2c})} \times\left[\pi\left(l+\frac{1}{2}\right)+\frac{3}{2}\sqrt{\frac{3}{4}}\right], \tag{42}$$

where

$$g(r_{2c}) = \frac{3\chi}{8k_c^2} \times\frac{2\sqrt{1+(r_{2c}/b)^n} - nF\left(1/2,\,-1/n,\,1-1/n,\,-(r_{2c}/b)^n\right)}{r_{2c}(n-2)}. \tag{43}$$

Here, F is a hypergeometric function. We use Equation (36) for the first turning point to obtain the above relation. The second turning point r_{2c} is given by the implicit relation $r_{2c} = [4k_c^2 r_2^2/(3\chi) - 1]^{1/n} b$ for $n > 2$. If $n \to \infty$, then we arrive at the case of the step-function profile. The hypergeometric function $F \to 1$ as $n \to \infty$ in Equation (42), and $r_{2c} \to b$. As a result, we again have a good approximation of

the known dispersion relation (Roberts et al. 1984). For the lower limit case $n = 2$, the second turning point r_{2c} is given by the explicit relation $r_{2c} = b/(4k_c^2b^2/(3\chi) - 1)^{1/2}$, while $r_{2c}F\left(1/2, 1/2, 3/2, -(r_{2c}/a)^2\right) = \ln\left(r_{2c}/b + \sqrt{(r_{2c}/b)^2 + 1}\right)$, and $g(r_{2c})$ is proportional to the same logarithmic function. It can be shown from Equation (42) that corresponding cutoff wave number is $k_cb \approx \sqrt{(3\chi)/4}$ for any radial order l. This value is slightly different from the exact expression given by Equation (30) due to the WKB approximation, but we confirm our previous result that all radial modes have the same cutoff in this case. When $0 < n < 2$, the second turning point tends to infinity. Then, by using the asymptotic expansion of the hypergeometric function (Abramowitz & Stegun 1970) for a large argument, we can write that $r_{2c}F(1/2, 1/n, 1 + 1/n, -(r_{2c}/a)^n) \propto r_{2c}^{1-n/2}$, and $g(r_{2c}) \propto k_c^{-2}r^{n/2-1}$. The right-hand side of Equation (42) tends to zero as $r \to \infty$, and we have $k_c \to 0$. This is in agreement with the results of Section 3.1.

Dispersion Equations (41) and (42) were solved numerically. In Figure 2, we displayed the dependence of cutoffs upon the indexes α and n for the fundamental, first, and second radial harmonics of pulsations. As expected, the cutoff wave numbers increase as α and n grow for both profiles. The cutoffs of each harmonic approach the same value as $n \to 2$ for the inverse polynomial profile, and tend to zero as $\alpha \to 0$ for the exponent-like profile.

3.2.2. Trapped Regime

The trapped wave regime ($m_e^2 = -n_e^2 < 0$) corresponds to

$$Q(r) = \left(k^2 - n_e^2\right)f(r) - n_e^2\chi - \frac{3\chi}{4r^2}. \quad (44)$$

There are two turning points for $Q(r)$, and the desired dispersion relation is given by Equation (37), where $Q_c(r)$ should be replaced by $Q(r)$. For the exponent-like profile function Equation (39), the first turning point can be expressed as $r_1^2 \approx (3/4)(\omega^2/V_{\rm Ai}^2 - k^2 + \omega^2/V_{\rm Ae}^2)^{-1}$, and $r_1 \ll a$ for all appropriate values of the phase speed $V_{\rm Ai} < V_{\rm ph} \leqslant V_{\rm Ae}$. The second one is given by the implicit relation

$$r_2 = \left(-\ln\left[\frac{\chi}{k^2 - n_e^2}\left(n_e^2 + \frac{3}{4r_2^2}\right)\right]\right)^{1/\alpha}a. \quad (45)$$

First, we consider the solution of dispersion Equation (37) for the wave numbers $k > k_c$, which are not much higher than the cutoff value. By using the Taylor series expansion on the small second and third terms of the integrand, we arrive at

$$\frac{V_{\rm ph}}{V_{\rm Ai}}ka - \frac{1}{2^{1/\alpha}\Gamma(1/\alpha)}\frac{n_e^2a^2}{\sqrt{n_e^2r_2^2 + 3/4}}\left(\frac{r_2}{a}\right)^{2-\alpha} \approx \frac{\alpha}{2^{1/\alpha}\Gamma(1/\alpha)}\left[\pi\left(l + \frac{1}{2}\right) + \frac{2 + \delta}{2\sqrt{\delta}}\sqrt{\frac{3}{4}}\right] \quad (46)$$

and the wave phase speed decreases as the wave number grows from the cutoff value. To evaluate the approximate solution of the dispersion Equation (37) for the short wavelength limit (large k), we apply the series expansion of the integrand, given that the last term is much smaller than the first and the second ones (see Equation (44)). Because $r_1/a \ll 1$ and $r_2/a < 1$ for $ka \gg 1$, the profile function Equation (39) can be approximated as $\exp\left[-(r/a)^\alpha\right] \approx 1 - (r/a)^\alpha$. We then obtain

$$\left(\frac{V_{\rm ph}^2}{V_{\rm Ai}^2} - 1\right)^{1/2}k(r_2 - r_1) + \frac{3}{8}\left(\frac{V_{\rm ph}^2}{V_{\rm Ai}^2} - 1\right)^{-1/2}k^{-1} \times \left(r_2^{-1} - r_1^{-1}\right) = \pi\left(l + \frac{1}{2}\right). \quad (47)$$

Equation (47) can be rewritten as

$$L + \frac{3}{8L}\frac{1}{k^2a^2} = \frac{1}{ka}\left[\pi\left(l + \frac{1}{2}\right) + \frac{3\sqrt{3}}{4}\right], \quad (48)$$

with

$$L = \left(\frac{V_{\rm ph}^2}{V_{\rm Ai}^2} - 1\right)^{1/2}\left(\frac{r_2}{a}\right). \quad (49)$$

For large ka, given that $r_2/a \approx \left(1 + \chi - V_{\rm Ai}^2/V_{\rm ph}^2\right)^{1/\alpha}$, we arrive at

$$V_{\rm ph}^2 \approx V_{\rm Ai}^2\left(1 + \left(\frac{c}{ka}\right)^{\frac{2\alpha}{\alpha+2}}\right),\ c = \pi\left(l + \frac{1}{2}\right) + \frac{3\sqrt{3}}{4}. \quad (50)$$

Equation (50) show that the phase speed of the fast sausage waves tends to the internal Alfvén speed in the short wavelength limit.

Obviously, the dispersion properties of the trapped mode for the inverse polynomial profile, given by Equation (29) with $n > 2$, are the same as that of the exponent-like profile. It is reasonable to study the dispersion features of sausage waves for the case $0 < n < 2$ given the results of Section 3.1, which indicate that the phase speed of the waves is below the external Alfvén speed for the entire range of wave numbers. The corresponding turning points are as follows: $r_1 \approx [3\chi V_{\rm Ae}^2/(4\omega^2b^2)]^{1/(2-n)}b$ and $r_2 \approx [\omega^2/(V_{\rm Ai}^2n_e^2) - 1]^{1/n}b$. First, taking into account that $r_1, r_2 \gg b$ for the long wavelength range, we use the series expansion of the integrand, given by Equation (44), on the small third term to evaluate the integral in Equation (37). The resulting dispersion equation reads

$$n_er_2 \approx d,\ d = \frac{4 - n^2}{3n + 2}\pi\left(l + \frac{1}{2} + \frac{1}{2 - n}\sqrt{\frac{3}{4}}\right). \quad (51)$$

Equation (51) gives an approximate solution of

$$V_{\rm ph}^2 \approx V_{\rm Ae}^2\left(1 - \frac{1}{2}\left(\frac{kb}{d}\right)^{\frac{2n}{2-n}}\chi^{-\frac{2}{2-n}}\right), \quad (52)$$

which is valid for $(kb/d)^n \ll \chi$. It can clearly be seen that the phase speed is below the external Alfvén speed even for $kb \ll 1$. In the short wavelength range (large k), it follows that $r_1^2 \approx (3V_{\rm Ai}^2/(4\omega^2)$, and both turning points $r_1, r_2 \ll 1$. Then we can use the Taylor expansion of the profile function for small argument r, and apply the same procedure as above to evaluate

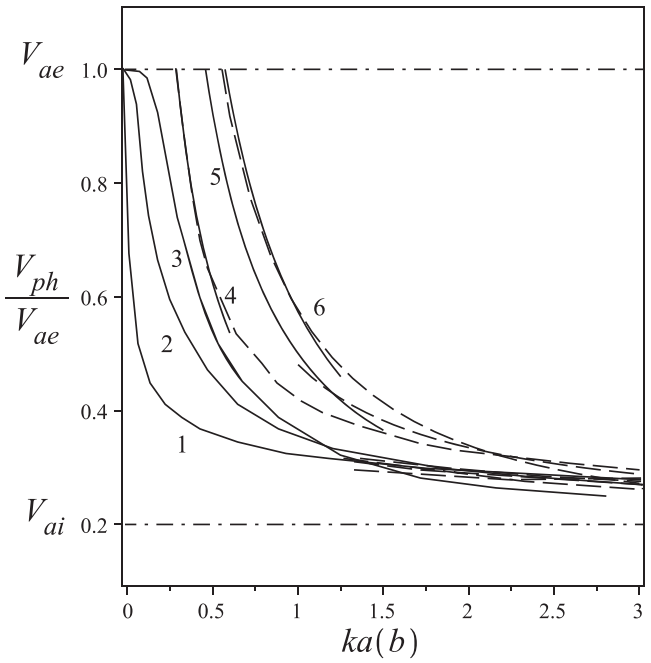

Figure 3. Dependence of the normalized phase speed of the fundamental fast-sausage mode against the normalized wave number $ka(b)$ for $V_{\rm Ae} = 5V_{\rm Ai}$. The curves 1, 2, and 3 correspond to the values of index $n = 1/2$, 1, and $3/2$, respectively. The curves, labeled as 4–6, correspond to the values of index $\alpha = 1$, 2, and 50, respectively. The solid and dashed lines are obtained on the basis of Equations (46), (51) and (48), (53), respectively.

the integral in Equation (37). After some algebra, we arrive at

$$\frac{\sqrt{\pi}}{2}\frac{\Gamma(1+1/n)}{\Gamma(3/2+1/n)}n_e b\left(\frac{r_2}{b}\right)^{n/2+1} - \frac{\sqrt{3}}{4}\left(\frac{r_2}{b}\right)^{-n/2} = \pi\left(l+\frac{1}{2}\right). \quad (53)$$

For a large wave number k, it follows that $n_e^2 \to k^2$, and Equation (53) can be simplified to the form

$$V_{\rm ph} \approx V_{\rm Ai}^2\left(1+\left(\frac{h}{kb}\right)^{\frac{n}{n+2}}\right),\ h = \sqrt{\frac{3}{4\pi}}\frac{\Gamma(3/2+1/n)}{\Gamma(1+1/n)}. \quad (54)$$

Figure 3 shows the dispersion curves for the fundamental fast-sausage mode ($l = 0$), obtained by the numerical solution of Equations (46), (48), (51), and (53) with $V_{\rm Ae} = 5V_{\rm Ai}$. It can clearly be seen that for an exponent-like density profile, the cutoff, wave number decreases with decreasing index α. The dispersion feature of the curves (viz. the parameter $dV_{\rm ph}/dk$) is weakly dependent on the index α. The phase speed tends to the internal Alfvén speed for large k, and the lower values of index α correspond to a slower decrease in $V_{\rm ph}$ with k (i.e., the lower value of parameter $dV_{\rm ph}/dk$), in accordance with Equation (50). Note that Equation (48), obtained for the short wavelength limit, is a good approximation of the dispersion relation for the entire range of wave numbers above the cutoff value. The dispersion curves for the inverse polynomial profile function with $0 < n < 2$ have no cutoff (see Equation (52)). The dispersion of the waves for the not too large wave numbers is highly sensitive to the value of index n. As $n \to 2$, the phase speed is near the external Alfvén speed up to the value of the wave number, given by Equation (30), and then tends to the internal Alfvén speed. For the indexes $n < 1$, the phase speed rapidly decreases from $V_{\rm Ae}$ at small values of the wave numbers kb, and then gradually tends to $V_{\rm Ai}$.

3.2.3. Leaky Regime

In the leaky wave regime ($m_e^2 > 0$), there is one turning point for $Q(r)$, and we can construct an appropriate solution of wave Equation (13) as follows:

$$\Xi_r(r) \approx [Q(r)]^{-1/4}A\exp\left[i\left(\frac{1}{\sqrt{\chi}}\int_{r_1}^{r}\sqrt{Q(y)}\,dy - \frac{\pi}{4}\right)\right], \quad (55)$$

where r_1 is a turning point and A is an arbitrary constant. On the other hand, the solution of wave Equation (13) at large distances from the tube axis can be expressed in terms of the Hankel function of the order of one:

$$\Xi_r(r) = Br^{1/2}H_1^{(1)}(m_e r) \approx B\left(\frac{2}{\pi m_e}\right)^{1/2}\exp\left[i\left(m_e r - \frac{\pi}{2} - \frac{\pi}{4}\right)\right]. \quad (56)$$

Obviously, the solutions given by Equations (55) and (56) must have the same functional form for large r. To satisfy this condition, we impose the next constraint

$$\frac{1}{\sqrt{\chi}}\int_{r_1}^{r}\sqrt{Q(y)}\,dy = m_e r + \pi\left(l+\frac{1}{2}\right). \quad (57)$$

Let us represent the integral in Equation (57) as

$$\frac{1}{\sqrt{\chi}}\int_{r_1}^{r}\sqrt{Q(y)}\,dy = \frac{1}{\sqrt{\chi}}\int_{r_1}^{r_2}\sqrt{Q(y)}\,dy + \frac{1}{\sqrt{\chi}}\int_{r_2}^{r}\sqrt{Q(y)}\,dy. \quad (58)$$

Here, r_2 is chosen in such a way that the r-dependent terms in the right-hand side of Equation (33) vanish for $r \geqslant r_2$. Then the second integral in Equation (58) can be approximated as

$$\frac{1}{\sqrt{\chi}}\int_{r_2}^{r}\sqrt{Q(y)}\,dy \approx m_e(r - r_2). \quad (59)$$

For the exponent-like profile function (see Equation (39)), the turning point is given by $r_1^2 = [(3V_{\rm Ai}^2)/(4\delta)]\omega^{-2}$, where δ is specified in Section 3.2.1., and we set $r_2 = (-\ln(\epsilon\chi))^{1/\alpha}a$, with $0 < \epsilon < 1$. To evaluate the first integral in Equation (58), we use the series expansion of the integrand, given that the first term in the right-hand side of Equation (33) is dominant for the interval $[r_1, r_2]$. With $ka \ll 1$, we obtain

$$\frac{1}{\sqrt{\chi}}\int_{r_1}^{r_2}\sqrt{Q(y)}\,dy \approx \frac{2^{1/\alpha}\Gamma(1/\alpha)}{\alpha} + \frac{1}{\alpha\sqrt{\epsilon}}\frac{\omega a}{V_{\rm Ae}}\left(\frac{r_2}{a}\right)^{1-\alpha} - \frac{2+\delta}{2\sqrt{\delta}}\sqrt{\frac{3}{4}}. \quad (60)$$

We can neglect the term $m_e r_2$ in Equation (59) and the second term in the right-hand side of Equation (60) because $\chi \ll 1$.

Then the resulting dispersion relation reads

$$V_{\rm ph} \approx \frac{\alpha}{2^{1/\alpha}\Gamma(1/\alpha)}\frac{V_{\rm Ai}}{ka}\left[\pi\left(l+\frac{1}{2}\right)+\frac{2+\delta}{2\sqrt{\delta}}\sqrt{\frac{3}{4}}\right]. \quad (61)$$

For the inverse polynomial profile function with $n > 2$ the turning point is $r_1^2 = [(3V_{\rm Ai}^2)/(4)]\omega^{-2}$, and we set $r_2 = (\epsilon\chi)^{-1/n}b$. By substituting Equation (29) into Equation (58) and applying the same procedure as for the exponent-like profile, we can obtain

$$\frac{1}{\sqrt{\chi}}\int_{r_1}^{r_2}\sqrt{Q(y)}\,dy \approx r_2 F\left(1/2,\, 1/n,\, 1+1/n,\, -(r_2/a)^n\right) \times \frac{\omega a}{V_{\rm Ai}} + \frac{1}{\sqrt{\epsilon}}\frac{\omega a}{V_{\rm Ae}}\left(\frac{r_2}{a}\right) - \frac{3}{2}\sqrt{\frac{3}{4}}. \quad (62)$$

Again, the term $m_e r_2$ in Equation (59) and the second term in the right-hand side of Equation (62) vanish because $\chi \ll 1$. As a result, we arrive at

$$V_{\rm ph} \approx \frac{\Gamma(1+1/n)\Gamma(1/2-1/n)}{\sqrt{\pi}}\frac{V_{\rm Ai}}{kb} \times\left[\pi\left(l+\frac{1}{2}\right)+\frac{3}{2}\sqrt{\frac{3}{4}}\right]. \quad (63)$$

It follows from Equations (61) and (63) that the phase speed infinitely grows as $ka(b) \to 0$. As $\alpha, n \to \infty$, both Equations (61) and (63) are good approximations for the leaky wave dispersion relation in the case of a step-function density profile (Meerson et al. 1978).

3.3. Seismological Application

There are a large number of reports concerning the analysis of observed QPPs in the solar flaring loops. However, of particular interest are the spatially resolved observations of pulsations with different periodicities. Kupriyanova et al. (2013) detected QPPs with several spectral components (at least three) in a solar flare on 2002 July 3, observed by the Nobeyama Radioheliograph (NoRH) with a high spatial resolution. The flaring loop length was estimated as $L = 35$ Mm and its minor radius as $a = 6.6$ Mm. The periods of QPPs are $P_1 \approx 31.1$ s, $P_2 \approx 18.7$ s, and $P_3 \approx 11.4$ s. The authors found that the P_1 component is most pronounced at the loop apex, while the P_2 component is most pronounced at the loop legs near its footpoints, and the P_3 component has three regions of high QPP amplitudes. These features allow us to interpret the observed pulsations in terms of the global, first, and second longitudinal harmonics of the MHD mode oscillations of the flaring loop, with corresponding normalized wave numbers $k_1 a \approx 0.59$, $k_2 a \approx 1.18$, and $k_3 a \approx 1.78$. The interpretation in terms of the fast-sausage mode in the model of coronal tubes with a discontinuous or steep boundary (i.e., $\alpha, n \gg 1$ for our profiles) has some complications. Indeed, at least the fundamental harmonic can be a leaky mode with significant damping in the case considered, until the density contrast is not too small. Besides, the fast-sausage mode is highly dispersive in the range of wave numbers above the cutoff value (see Figure 3), and the corresponding phase speed of the global and second longitudinal modes should be significantly different. These properties, however, contradict the observational results. Alternatively, we suggest using the model of loops with a smooth boundary, either with the exponent-like density profile and a not too large value of the index α, or with the inverse polynomial density profile, where the decrease of the density from the tube axis is slower than r^{-2} (i.e., $0 < n < 2$). The most correct results are obtained on the basis of Equation (51) for the inverse polynomial approximation of the transverse density profile with index $n \approx 0.85 - 1.20$. The estimates of the density contrast are in the range $\chi \approx 0.07 - 0.27$ and the Alfvén speed outside the loop $V_{\rm Ae} \approx 2.6 - 4.3\,{\rm Mm\,s^{-1}}$. The corresponding oscillation periods are 30.8–31.4 s, 18.4–18.9 s, and 13.5 s. On the other hand, the exponent-like model of the profile function supports the existence of the trapped global fast-sausage mode because the cutoff wave number decreases with decreasing index α, but the modes considered remain highly dispersive and cannot provide the observed ratios of periodicities.

We also consider the long-period multiple sausage oscillations detected in a large and cool postflare loop in the 2001 May 2 flare event reported by Srivastava et al. (2008). The estimated loop length is $L \approx 100$ Mm, and its width $a \approx 3$ Mm. The periods of the spectral components are $P_1 \approx 587$ s and $P_2 \approx 349$ s. These oscillations were interpreted in terms of the fundamental and first longitudinal harmonics of fast-sausage waves in the postflare loop. The corresponding normalized wave numbers of the detected modes are $k_1 a \approx 0.09$ and $k_2 a \approx 0.19$, while their phase speed $V_{\rm ph1} \approx 340\,{\rm Km\,s^{-1}}$ and $V_{\rm ph2} \approx 286\,{\rm Km\,s^{-1}}$. The authors' estimates, based on the theory of the sausage mode in tubes with a step-function density profile, lead to the restriction of the density ratio to >600, to realize a case of a trapped global mode with the observed period and calculated wave number. The deviation of the observed period ratio of modes $P_1/P_2 \approx 1.68$ from 2 is attributed by authors to the longitudinal density stratification inside the loop. However, it should be noted that the effect of longitudinal density stratification produces a significant shift of period ratio from 2 only for the fundamental fast kink mode, with its almost constant phase speed at a long wavelength limit. (Andries et al. 2005; McEwan et al. 2006). For the sausage modes, the dispersion provides an excessive shift of the period ratio to explain the observed values (Macnamara & Roberts 2011). We applied the results of the present paper to the above observations. We could not find any acceptable combination of parameters in the model of an exponent-like density profile (i.e., χ, $V_{\rm Ae}$, and α) because the dispersion curves, in this case, have a too large gradient in the cutoff region. This feature is clearly seen in the behavior of curves 4–6 in Figure 3. Nevertheless, the quite small value of $k_1 a \approx 0.09$, identified by the cutoff wave number, can be easily obtained in this model with the parameter $\alpha \lesssim 1$, and for a density ratio <150. We do not consider here too small values of α, since they correspond to a situation where the bulk of the plasma material is concentrated in the vicinity of the loop axis. On the other hand, curves 2 and 3 in Figure 3 have the most appropriate dispersion properties to explain the observation analyzed. These curves are calculated for the inverse polynomial profile function with indexes $n = 1$ and $3/2$, and they have rather minor gradients in the range of small wave numbers. Besides, in this case, the waves are trapped for all wave numbers. When using Equation (51), we now have three unknown parameters χ, $V_{\rm Ae}$, n, and two equations containing the phase speed of both modes. We found the following set of estimates: $V_{\rm Ae} \approx 380\,{\rm km\,s^{-1}}$ and $\chi \approx 0.060$ for index $n = 1$,

$V_{Ae} \approx 345$ km s^{-1} and $\chi \approx 0.030$ for $n = 1.5$, and $V_{Ae} \approx 340$ km s^{-1} and $\chi \approx 0.014$ for $n \approx 2$. For this plasma characteristic, we obtained the most correct values of the measured phase speed of the observed harmonics.

4. CONCLUSIONS

We examined the fast-sausage waves in monolithic coronal tubes with a smooth radial density distribution. The low-β plasma tube was represented as the density enhancement, described by the continuous profile function $f(r)$. In order to derive the criteria, determining the existence of trapped or leaky modes as a function of the profile features, we applied Kneser's oscillation theorem to the wave equation. The results obtained were supplemented by analytic solutions to the original wave equation for the particular cases of the profile function. The WKB method allowed us to determine the approximate dispersion relations for the entire range of longitudinal wave numbers. We summarize our findings as follows.

1. The monolithic coronal tubes with a radial density profile which decreases slower than r^{-2} support only trapped fast-sausage modes over the whole range of the longitudinal wavelength. If the density decreases like r^{-2} at large distances from the tube axis, then the fast-sausage modes of any transverse order l have the same cutoff wave number. All other profile functions $f(r)$ which decrease faster than r^{-2} at large distances r lead to an infinite number of cutoffs. In the last case, there are both trapped and leaky modes.
2. For the inverse polynomial profile function with index $n > 2$, and an exponent-like profile function with arbitrary index α, the corresponding values of the cutoff wave numbers decrease as the tube boundary becomes less steep (i.e., as indexes n and α decrease).
3. The behavior of the dispersion curves for the inverse polynomial profile function with $0 < n < 2$ is highly sensitive to the value of the index n in the range of not too large wave numbers. As $n \to 2$, the phase speed is near the external Alfvén speed up to a certain value of the wave number, given by Equation (30), and then tends to the internal Alfvén speed. For the indexes $n < 1$, the phase speed rapidly decreases from the V_{Ae} value in the range of small wave numbers kb, and then gradually tends to the V_{Ai}.
   The dispersion features of fast-sausage waves in the trapped regime are weakly dependent on the indexes n and α for the inverse polynomial profile function with $n > 2$ and the exponent-like profile function with an arbitrary index α. The most pronounced feature is the dependence of cutoff wave numbers on the parameters n and α, as discussed above.
4. The phase speed of waves in the leaky regime (wave numbers below the cutoff value) is inversely proportional to the wave number k and infinitely grows as $k \to 0$.
5. The seismological application of the results obtained shows that the approximation of the transverse density profile in the flaring loop by the inverse polynomial profile function with $n \approx 0.8$–2 can quite adequately explain the observed multiperiodicities in QPPs and the corresponding ratios of the periods. The estimated values of the external Alfvén speed V_{Ae} and density contrast χ lie in the range 2.6–4.3 Mm s^{-1} and 0.07–0.27, respectively, for the 2002 July 3 flare. The corresponding estimates for the cool postflare loop of the 2001 May 2 event have the following values: $V_{Ae} \approx$ 0.34–0.38 Mm s^{-1} and $\chi \approx 0.01$–0.06.

The results obtained clearly indicate that transverse density structuring in coronal waveguides can affect the dispersion properties of fast-sausage modes, and this finding should be taken into account in the analysis of observed QPPs in the flare events and sausage wave propagation in solar magnetic tubes.

We thank the anonymous referee for useful suggestions. This work was supported by the Russian Science Foundation (agreement 14-50-00034). The theoretical investigation was carried out at the Ussuriisk astrophysical observatory. The numerical calculations were made at the Far Eastern Federal University.

REFERENCES

Abramowitz, M., & Stegun, I. A. (ed.) 1970, in Handbookof Mathematical Functions: With Formulas, Graphs, and Mathematical Tables (New York: Dover), 379
Andries, J., Arregui, I., & Goossens, M. 2005, ApJL, 624, L57
Appert, K., Gruber, R., & Vaclavik, J. 1974, PhFl, 17, 1471
Bender, C. M., & Orszag, S. A. 1978, Advanced Mathematical Methods for Scientists and Engineers (New York: McGraw-Hill)
Cally, P. S. 1986, SoPh, 103, 277
Cooper, F. C., Nakariakov, V. M., & Williams, D. R. 2003, A&A, 409, 325
Edwin, P. M., & Roberts, B. 1983, SoPh, 88, 179
Edwin, P. M., & Roberts, B. 1988, A&A, 192, 343
Goossens, M., Andries, J., & Arregui, I. 2006, RSPTA, 364, 433
Goossens, M., Andries, J., & Aschwanden, M. 2002, A&A, 394, L39
Goossens, M., Terradas, J., Andries, J., Arregui, I., & Ballester, J. L. 2009, A&A, 503, 213
Hornsey, C., Nakariakov, V. M., & Fludra, A. 2014, A&A, 567, 24
Kahn, P. B. 1990, Mathematical Methods for Scientists and Engineers (New York: Wiley)
Khongorova, O. V., Mikhalyaev, B. B., & Ruderman, M. S. 2012, SoPh, 280, 153
Kneser, A. 1893, MatAn, 42, 409
Kopylova, Y. G., Melnikov, A. V., Stepanov, A. V., Tsap, Y. T., & Goldvarg, T. B. 2007, AstL, 33, 706
Kupriyanova, E. G., Melnikov, V. F., & Shibasaki, K. 2013, SoPh, 284, 559
Lopin, I., & Nagorny, I. 2013, ApJ, 774, 121
Lopin, I. P., & Nagorny, I. G. 2014, A&A, 572, 60
Lopin, I. P., & Nagorny, I. G. 2015, ApJ, 801, 23
Macnamara, C. K., & Roberts, B. 2011, A&A, 526, A75
McEwan, M. P., Donnelly, G. R., Díaz, A. J., & Roberts, B. 2006, A&A, 460, 893
Meerson, B. I., Sasorov, P. V., & Stepanov, A. V. 1978, SoPh, 58, 165
Melnikov, V. F., Reznikova, V. E., Shibasaki, K., & Nakariakov, V. M. 2005, A&A, 439, 727
Moreels, M. G., Goossens, M., & Van Doorsselaere, T. 2013, A&A, 555, A75
Musielak, Z. E., & Moore, R. L. 1995, ApJ, 452, 434
Nakariakov, V. M., Hornsey, C., & Melnikov, V. F. 2012, ApJ, 761, 134
Nakariakov, V. M., & Melnikov, V. F. 2009, SSRv, 149, 119
Nakariakov, V. M., Melnikov, V. F., & Reznikova, V. E. 2003, A&A, 412, L7
Nakariakov, V. M., & Roberts, B. 1995, SoPh, 159, 399
Roberts, B., Edwin, P. M., & Benz, A. O. 1984, ApJ, 279, 857
Rosenberg, H. 1970, A&A, 9, 159
Ruderman, M., & Roberts, B. 2002, ApJ, 577, 475
Sakurai, T., Goossens, M., & Hollweg, J. V. 1991, SoPh, 133, 227
Schmitz, F., & Fleck, B. 1998, A&A, 337, 487
Spruit, H. C. 1982, SoPh, 75, 3
Srivastava, A. K., & Goossens, M. 2013, ApJ, 777, 17
Srivastava, A. K., Zaqarashvili, T. V., Uddin, W., Dwivedi, B. N., & Kumar, P. 2008, MNRAS, 388, 1899
Vasheghani Farahani, S., Hornsey, C., Van Doorsselaere, T., & Goossens, M. 2014, ApJ, 781, 92
Zaitsev, V. V., & Stepanov, A. V. 1975, IGAFS, 37, 3
Zaitsev, V. V., & Stepanov, A. V. 1982, SvAL, 8, 132